Damage Evaluation of RC Bridge Deck under Wheel Loading Test by Means of AE Tomography

Takahiro Nishida[1)], Tomoki Shiotani[1)], Hisafumi Asaue[1)], Takuya Maejima[2)], Yoshikazu Kobayashi[3)]
1) Kyoto University, C3-b4S16, Nishikyo-ku, Kyoto, 615-8540, Japan.
2) Nihon University, Nihon University, Koriyama, Fukushima, 963-8642, Japan.
3) Nihon University, Nihon University, 1-8-14, Kanda-Surugadai, Chiyoda-ku, Tokyo, 101-830, Japan.

ABSTRACT: Remediation and replacement of deteriorated reinforced concrete (RC) bridge decks are severely concerned in Japan, and thus intensive studies for long-term operation of the decks are recently carried out. For implementing proper remediation program of the deck, damage evolution should be evaluated in advance. So far, damage grading has been conducted from crack patterns by naked eyes. This kind of visual investigation is well implemented for the correcting maintenance procedure, where the repair shall be conducted when the remarkable deterioration is found on the surface of the deck. However, to reduce the repair budget, leading to the decrease in the amount of road investment as well as life-cycle cost, the deterioration and damage should be evaluated before being visually identified on the surface. To this end, internal damage of RC decks due to fatigue is reproduced experimentally by wheel-loading apparatus. Then, the damage progress is quantitatively and visually evaluated by AE tomography analysis.

1 INTRODUCTION

Among road investment, large share has been reported for the bridge-deck replacement. Conventionally, fatigue damage has been discussed when the deterioration becomes remarkable as to be observed on the surface of the deck. So far, characteristics of surface cracks on the directions and the densities have been employed to determine the grade of the damage in the deck due to fatigue. This kind of visual investigation is well implemented for the correcting maintenance procedure, where the repair shall be conducted when the remarkable deterioration is identified on the surface.

In order to reduce the repair budget, leading to the decrease in the amount of road investment as well as life-cycle cost, deterioration and damage are preferably to be evaluated before being identified on the surface of the deck [1]. Bridge owners have long been wondering whether the investment might be reduced as internal damage is properly evaluated with nondestructive testing (NDT) approaches and the damage is reasonably quantified. To detect internal damage, the elastic wave tomography and AE tomography [2][3] are under development. As well known, X-ray tomography [4] is only one tool to visualize the internal damage, while it costs a lot and is time-consuming, in addition to bringing harmful situation against human health.

AE measurements are known to be effective to trace the damage continuously [5]. However, to locate AE sources, a multi-channel system is necessary. Thus, practical applications are even limited to important structures only. In addition, external environmental noises are problematic for that long-term monitoring on site. Therefore, real-time fatigue damage monitoring with AE technique has been conducted for experimental purposes [6].

In contrast to AE monitoring, signal excitation and detection are performed in ultrasonics, as at least one pair of input and output sensors are applied to explore internal damages. Locations of defects are estimated from propagation time, by assuming unique or spatially homogeneous velocity of ultrasonic wave. In the case that the wave-propagation length of the media is known, overall deterioration can be estimated from the wave-velocity calculated with propagation time. Also it is noted that AE source location is useful for evaluating damage positions/ areas. In the case, the wave-velocity is necessarily determined in advance, because the sources are located on the basis of arrival-time differences among sensors, assuming the unique velocity value.

Innovative AE tomography has been developed [3][8] for more than a decade, being able to determine the both of wave-velocity and AE sources even under the condition that the damage is evolving or exists within the materials of interest.

In this study, the fatigue evolution in RC decks is reproduced by wheel-loading apparatus. Three-dimensional (3D) AE tomography analysis is executed at proper periods through the test. Thus, internal progress of fatigue damage is visualized and quantified from distribution of the elastic-wave velocities, taking into account surface cracks observed.

2 WHEEL LOADING PROGRAM

To induce fatigue failure to an RC deck specimen, repeated loading with a steel wheel was conducted. The specimen is a plate of dimensions 3000 ×2000 ×210 mm, with steel reinforcement arranged as shown in Fig. 1. A steel wheel of 300 mm in diameter and 400 mm in width can be applied with the load up to 250 kN in the case of repeated loading and 534 kN in the case of static loading. In order to generate crack patterns actually observed in the decks, being different from the conventional wheel-loading apparatus, a movable loading-wheel [7] was developed on the

foundation. The wheel can move horizontally from ±500 mm to ±1000 mm. The repetition rate is to be set between 0.897 - 9.97 rpm/ min The motion of ±500 mm and the rate 8.97 rpm were applied to the test.
Here, step-wise cyclic loadings are performed as show in Fig. 2. In the 1st cycles, the load of 98 kN was repeatedly applied $100x10^3$ times, and then elastic-wave excitations were applied by using a steel-hammer of 35mm diameter for 3D AE tomography. In the 2nd cycles, then, the load of 127.4 kN were applied $200x10^3$ times. Again, elastic-wave excitations were performed after this loading step. The 3rd cyclic loadings were conducted $250x10^3$ times with 156.8 kN load, prior to the elastic-wave excitations. It is noted that the specimen reached the fatigue limit at $235x10^3$th loading step.

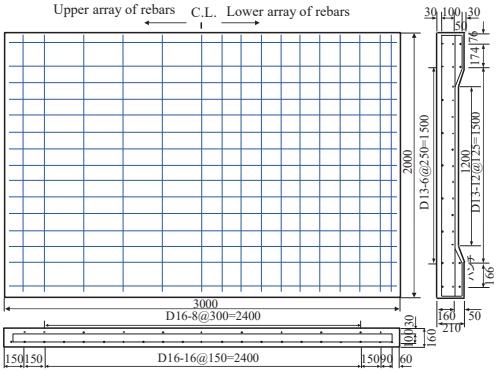

Fig. 1 Configuration of RC deck specimen (unit: mm).

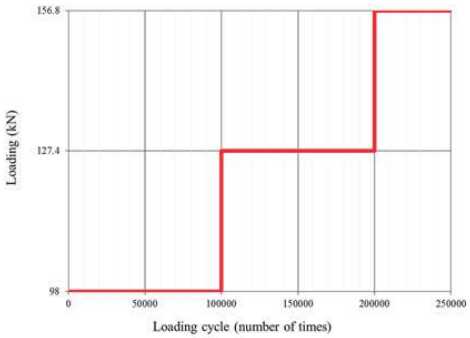

Fig. 2 Loading levels repeated in wheel-loading test.

3 MEASURING CONDITIONS

Damage evolution could be visualized, plotting AE sources accumulated through the whole failure process. In structures in service, however, it is not easy to install AE sensors in defective conditions. Therefore, the tomography analysis is applied by employing elastic-wave excitations. As illustrated in Fig. 3, 32 AE sensors of 60 kHz resonant are placed at 10 locations on the top, 18 locations on the bottom and 2 each on the two sides. The excitations were driven by a hammer of 35 mm diameter at designated 18 locations on the top and 22 on the bottom surface. The wheel loadings were applied in the longitudinal direction, at the area between green lines in Fig. 3. During the load holding in Fig. 2, vertical loads were applied vertically at the central
area denoted by a red rectangle.
Elastic-wave signals generated due to the excitations were amplified at the sensor-integrated pre-amplifier by 40 dB and recorded in AE monitoring system, of 48-channel with a 16 bit A/D conversion rate and 1 MHz sampling rate.

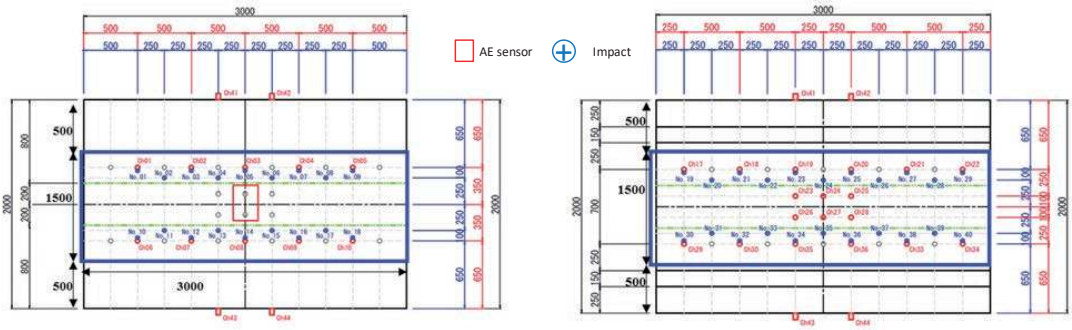

(a) Upper surface (unit: mm) (b) Bottom surface (unit: mm)

Fig. 3 Locations of AE sensors and impact points with loading areas.

4 THEORY OF AE TOMOGRAPHY

In AE tomography (hereafter referred to as AET), both of source locations and velocity distribution are simultaneously calculated. Here, the source location algorithm developed is briefly explained. Detailed tomographic procedure is to be referred to the other literature [8].
The location technique is based on the ray-trace algorithm [9], where relay points are assigned in each cell as illustrated in Fig. 4. Since the ray-paths are formed, connecting with segments among nodal points, its resolution depends on the mesh size. Namely, the high accuracy of source locations requires the finer mesh. This leads to the

increase in the number of degrees of freedom since the slowness, a reciprocal of velocity, shall be defined in each cell. In the ray-trace algorithm proposed, the relay points between the nodes are taken into account and then a new ray-path is formed with segments among the nodal points and relay points as shown in Fig. 5. As a result, the resolution of ray-trace is increased without the increase in the degrees of freedom. Because of the role of the relay points, relaying the signals, the relay points shall be distributed uniformly in the space. However, a non-uniform shape of cross section in a concrete structure does not allow uniform distribution of the relay points. To solve this problem, the relay points are installed by using iso-parametric mapping in the ray-trace algorithm. Since each cell is mapped onto an isosceles-right triangle, the relay points are uniformly installed in the mapped cell as shown in Fig. 6. This algorithm does not give exactly uniform distribution of the relay points in the case that the shape of the cell is skewed. Avoiding strongly skewed cells, the distribution of the relay points is improved and the source location is performed by applying this ray-trace algorithm. The procedure is briefly summarized in Fig. 7. The ray-traces are generated from a receiver as illustrated in Fig. 8. Travel times t_{ij} from receiver i to all nodal and relay points j are calculated. Since arrival time T_i at receiver i is estimated in the experiment, the possible emission time of the signal E_{ij} is computed by Eq. 1 at a nodal or relay point j.

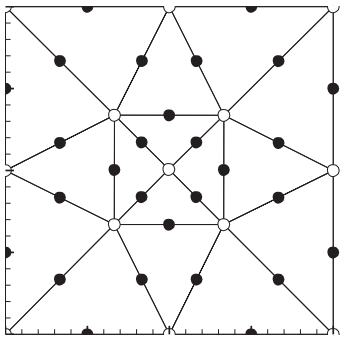

Fig. 4 Conventional set of relay points.

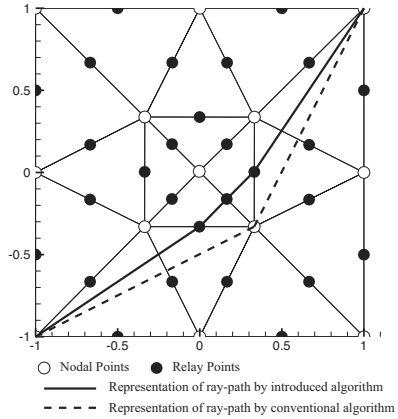

Fig. 5 Revised ray path in consideration of proposed relay points.

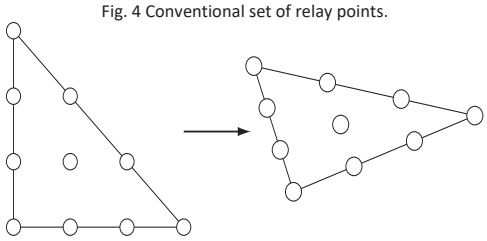

Fig. 6 Mapping to the global coordinate of set relay points.

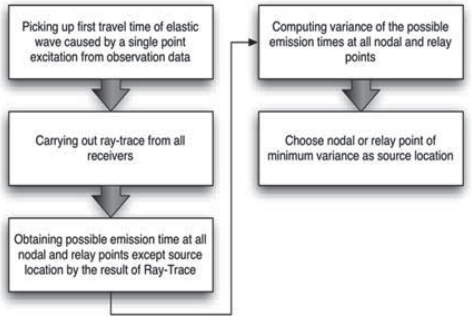

Fig. 7 Procedure to estimate the source locations.

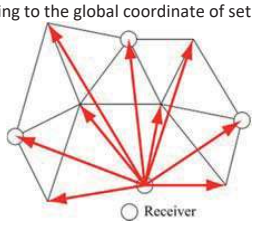

Fig. 8 Mapping to the global coordinate of set relay points

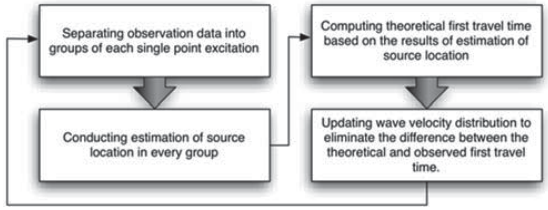

Fig. 9 Procedure to estimate the source locations and velocity distributions

$$E_{ij} = T_i - t_{ij} \qquad (1)$$

The step is applied to all receivers, and then the variance of the E_{ij} is computed as follow.

$$\sigma_j = \frac{\sum_i (E_{ij} - m_j)^2}{N} \qquad (2)$$

in which

$$m_j = \frac{\sum_i E_{ij}}{N} \qquad (3)$$

where N is the number of receivers.
For the estimation of the source location, the variance σ_j is evaluated. If distribution of the slowness is identical to that of the real slowness, σ_j must be equal to zero at the source location and m_j must be exactly the emission time. Due to the discretization error of slowness distribution and insufficient resolution of ray-trace, generally σ_j is not equal to zero. Still, it is reasonably considered that σ_j could be the minimum. Hence, the source locations are to be determined as the nodal or relay points of the minimum variance $\sigma_{j\,\min}$. Additionally, m_j is referred to as the possible emission time. It is noted that the accuracy of the source locations is controlled by the density of nodal and relay points because the source locations are assigned to a nodal or relay points in the proposed algorithm. Furthermore, by applying this technique to the iterative procedure on the identification of a wave-velocity structure, the source locations are updated in every iterative step, improving the accuracy of the source location. This approach can be applied to not only AE signals but also signals that are generated by elastic-wave excitations. Although the conventional tomography requires locations of sources, emission times and travel times to the receiver, source locations and emission times can be estimated from travel times to the receivers in the wave velocity distribution determined. Based on these facts, a tomographic procedure with estimation of source locations is developed and summarized in Fig. 9. In the first step, the source location and emission time are estimated. Here, the observed travel times are to be separated into groups, respectively, that are associated with individual excitation points. The source location and emission time are estimated for each travel-time group observed. In the second step, the ray-traces to all estimated source locations are calculated. Since the ray-traces are made for the all of estimated source locations, the travel times among the estimated source locations and the other nodal or relay points are derived. Eventually, theoretical travel times at receivers are obtained, given by adding the computed travel time t_{ij} to the estimated emission time m_j,

$$T_i' = m_j + t_{ij} \qquad (4)$$

In the third step, the slowness distribution is updated to eliminate the difference between the theoretical travel time and observed.
Recently, two-dimensional AE tomography (2D AET) mentioned above is upgraded into 3D AET [8]. The most difference between 2D AET and 3D AET is the ray-trace technique in the algorism. In the ray-trace technique, the waves in 3D AET are expressed in Eqs. 5 and 6, which are to be expanded to 3D from Eq. 7 in 2D AET.

$$a_1x + b_1y + c_1z + d_1 = 0 \qquad (5)$$
$$a_2x + b_2y + c_2z + d_2 = 0 \qquad (6)$$
$$ax + by + c = 0 \qquad (7)$$

In the following, 3D AET is applied to the RC deck specimen damaged by the wheel-loading.

5 RESULTS OF 3D AET

In order to estimation of velocity distributions after loading times of $100\text{x}10^3$, $200\text{x}\ 10^3$, and $250\text{x}10^3$, the target area (blue rectangular in Fig.3) for 3D AET analysis is divided into rectangular-parallelepiped cells, which consist of 25 (long axis direction) ×11 (short axis direction) ×5 (thickness direction) nodes. Results of 3D AET after three loading phases are given in Figs. 10, 11, and 12. After $100\ \text{x}10^3$ times loading, the velocity distributions are almost identical inside the specimen as shown in Fig. 10(a)-(d). The overall velocity is approximately 3500 m/s. It is found from the three-dimensional model in Fig. 10(d) that the velocity in the right side of the specimen tends to be lower. Following $200\text{x}10^3$ times loading, a low velocity zone appears as illustrated in Fig. 11(a)-(d). The velocity of right side on the surface is of slower velocity than 3000 m/s. From Fig. 11 (d), it is realized that internal velocity distribution is not homogeneous as the previous stage. This implies a state in which soundness and fatigue damage parts are mixed up. Velocity distributions after $250\text{x}10^3$ times are shown in Fig. 12(a)-(d). During this loading phase the specimen actually reached to the fatigue limit. The zones of the velocity lower than 2500 m/s extensively appear in the whole of specimen. Comparing with the velocity distributions after $100\text{x}10^3$ and $200\text{x}10^3$ times, the velocities drastically decrease. Low velocity zones could be particularly identified at wheel-running areas, suggesting the severe damage.

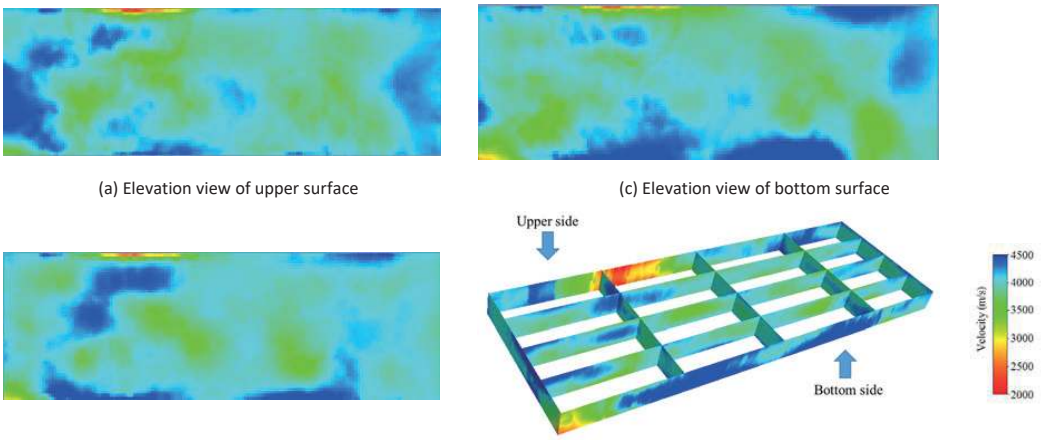

(a) Elevation view of upper surface (c) Elevation view of bottom surface

(b) Elevation view at middle depth (d) Three-dimensional model

Fig. 10 Velocity distributions of RC specimen after $100x10^3$ times loading.

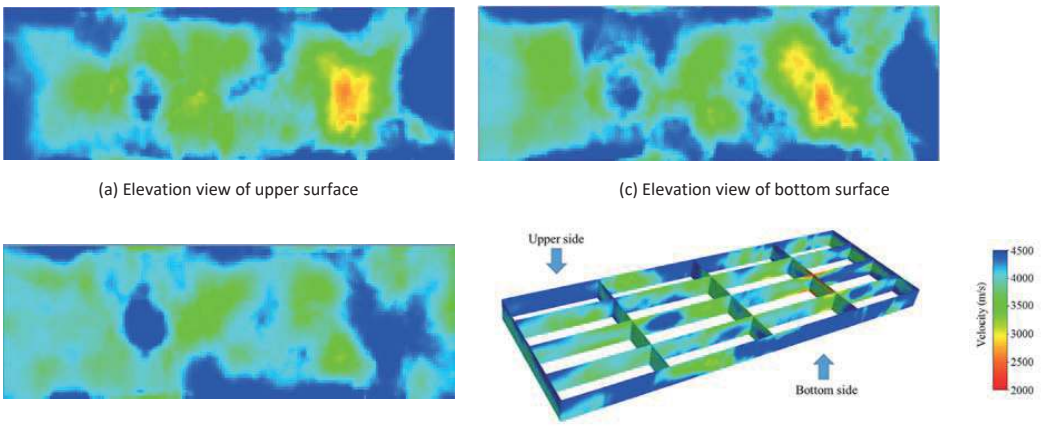

(a) Elevation view of upper surface (c) Elevation view of bottom surface

(b) Elevation view at middle depth (d) Three-dimensional model

Fig. 11 Velocity distributions of RC specimen after $200x10^3$ times loading.

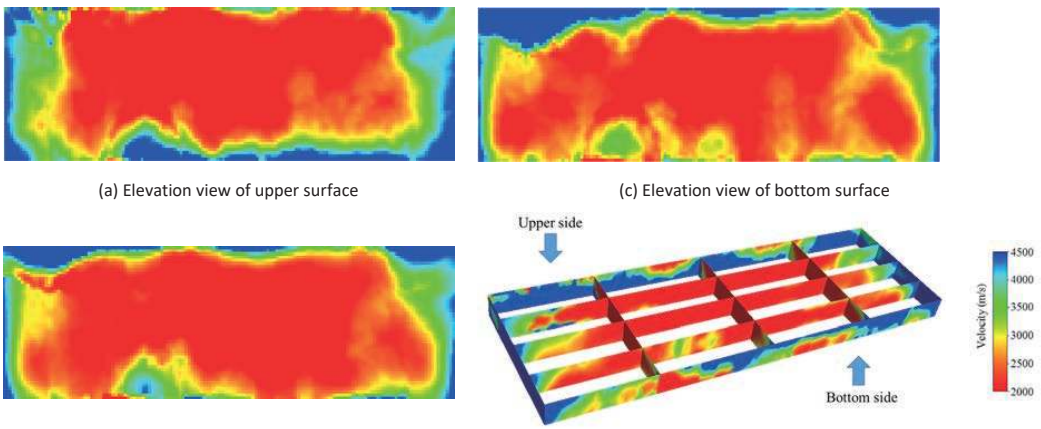

(a) Elevation view of upper surface (c) Elevation view of bottom surface

(b) Elevation view at middle depth (d) Three-dimensional model

Fig. 12 Velocity distributions of RC specimen after $250x10^3$ times loading.

6 DISCUSSIONS

Cracks distributions observed at the bottom are shown in Fig. 13(a)-(c). After the loading of $100x10^3$ times, many cracks are observed at the central area, and they are densely distributed in the right side. Although the lower velocities are identified (Fig. 10 (c)) in the densely cracked area, they are not particularly low. Thus, fatigue damage is considered to be severe at this stage. In comparison of crack distribution after $200x10^3$ times with that after

$100x10^3$ times, densely cracked areas are found in the center and right portions. The fact clearly reflects the velocity structure in Fig. 11 (c). The lower velocity zone than 3000 m/s exists on the right side. It is considered that the fatigue failure could start around. This suggests that the progress of fatigue failure is associated with not only the intensity of the load, but also the variation in the quality of concrete placement.
Cracks and the velocity areas lower than 2700 m/s distribute all over the bottom side after loading of $250x10^3$ times. The low velocity areas are clearly confirmed in Fig. 12(a)-(d), surely reflecting deterioration by fatigue damage. In addition, the velocity change rate from $200x10^3$ to $250x10^3$ times was more rapidly than that from $100x10^3$ to $200x10^3$ times. According to this study, the application of 3D AET to real RC decks is promising to carry out the preventive maintenance effectively.

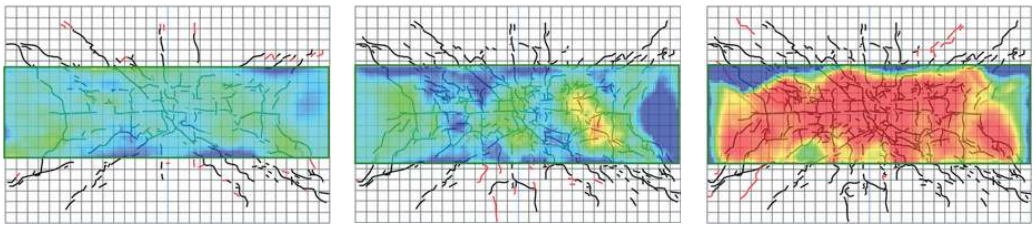

(a) 100 $x10^3$ times (b) 200 $x10^3$ times (c) 250 $x10^3$ times (after fatigue limit)
Fig. 13 Overlay map on the bottom surface by velocity distribution and clack situation.

7 CONCLUSIONS

3D AET is applied to a quantitative study on internal fatigue damage of RC deck. The damage was reproduced by the wheel-loading apparatus and tomographic analyses are conducted at three loading phases. With the tomographic approach, it is clearly demonstrated that internal velocity-distributions change in the RC deck specimen due to fatigue loading. Since the decrease in the velocities of RC decks suggest the generation of internal cracks, damaged areas are to be identified by 3D AET visually. Thus, progress of fatigue damage in RC decks is readily inspected by this procedure.

ACKNOWLEDGEMENTS

In this study, experiments were mostly conducted in College of Engineering of Nihon University under support of Cross-Ministerial Strategic Innovation Promotion Program (SIP). The authors wish to thank Prof. I. Iwaki and Associate Prof. Y. Koda of Nihon University as well as Associate Prof. Y. Tanaka of The University of Tokyo.

REFERENCES

[1] D. Frangopol, K. Lin and A. Estes, 'Life-Cycle Cost Design of Deteriorating Structures', ASCE, J. Struct. Eng., 0733-9445(1997)123:10(1390), pp. 1390-1401, 1997.
[2] Y. Kobayashi, T. Shiotani and H. Shiojiri, 'Damage identification using seismic travel time
[3] tomography on the basis of evolutional wave velocity distribution model', Engineering Technics Press, Proceedings of Structural Faults and Repair 2006, 2006 (CD-ROM).
[4] T. Shiotani, S. Osawa, S. Momoki and H. Ohtsu, 'Visualization of damage in RC bridge deck for bullet trains with AE tomography', Springer, Advances in Acoustic Emission Technology, pp. 357-368, 2014.
[5] J. Otani and Y. Obara edts, 'X-ray CT for geomaterials, soils, concrete, rocks', A.A. Balkema, 2004.
[6] U. Grosse & M. Ohtsu edts, 'Acoustic Emission Testing', Springer, 2008.
[7] T. Shiotani, D.G. Aggelis and O. Makishima, 'Global monitoring of large concrete structures using acoustic emission and ultrasonic techniques: case study', ASCE, J.Bridge Eng., Vol. 14, No. 3, pp. 188-192, 2009.
[8] T. Shiotani, H. Ohtsu, S. Momoki, HK. Chai, H. Onishi and T. Kamada, 'Damage evaluation for concrete bridge deck by means of stress wave techniques', ASCE, J. Bridge Eng., Vol.17, No. 6, pp. 847-856, 2012.
[9] T. Shiotani, S. Osawa, Y. Kobayashi and S. Momoki, 'Application of 3D AE tomography for triaxial tests of rocky specimens', Proceedings of 31st conference of the European Working Group on Acoustic Emission (EWGAE), 2014 (CD-ROM).
[10] F. Schubert, 'Basic principles of acoustic emission tomography', Journal of Acoustic Emission, 22, pp. 147-158, 2004.